Proceedings of ASME Turbo Expo 2011
GT2011
June 6-10, 2011, Vancouver, British Columbia, Canada

GT2011-46113

VISCOUS CONTROLLED VORTEX DESIGN OF A 1.5-STAGE AXIAL SUBSONIC TEST TURBINE

Qingfeng Deng, Qun Zheng, Chunlei Liu, Hai Zhang and Mingcong Luo
(College of Power and Energy Engineering, Harbin Engineering University, Harbin 150001, China)
E-mail: zhengqun@hrbeu.edu.cn, dengqingfeng@hrbeu.edu.cn

ABSTRACT

This paper presents a Viscous Controlled Vortex (VCV) design practice of an experimental turbine. The Controlled Vortex (CV) design method was modified to take the local viscous losses into account. The method began with the analysis of initial turbine geometry of a 1.5-stage turbine, which was designed by a developed CV design approach based on a prescribed pressure distribution to resolve the circulation requirements. Then the loss corrections were combined into the terms of the CV design equations and the pressure distributions are refined. The design and optimization of the 1.5-stage axial test turbine demonstrates the effectiveness of this technique. A reduction of secondary flows and a corresponding increase of stage efficiency have achieved.

Keywords: Turbine design; Viscous controlled vortex design method; Numerical simulation.

INTRODUCTION

The so called Controlled Vortex (CV) design method is a technique that radial distribution of work extraction and reaction is alterable relative to Free Vortex (FV) design. This method gives the designers a great versatility in design to fully develop the work capacity done by blades, which resulted in the present CV design system. CV design can also be termed the Non-Free Vortex (NFV) design relative to FV design. Comparative computational investigations had been carried out by Vad et al [1] on two axial flow pump rotors of FV and NFV design. The results of simulation showed that NFV design is an effectual method for increase of specific performance and offers a potential to avoid highly twisted blades. Some papers published measurement results on axial flow fans of NFV design [2] [3]. The researches were determined to develop flow pattern in the axial flow fans, the structure of secondary flow due to NFV operation was studied in detail. Conceptual optimization of axial-flow hydraulic turbines with NFV design was conducted by Albuquerque et al [4]. The comparison with the original turbine design showed potential performance improvements. CV design method has many other possible applications to extract non-uniform work from the stream, preventing mixing losses and providing uniform exit properties. The example case described in reference [5] exhibited that the best inlet tangential velocity profile is a fourth order polynomial and a 3.46% loss of stagnation pressure is prevented.

The CV design method is considered satisfactory. However, the method is an essential non-viscous technique. The weakness of the above procedure is that it neglects the viscous effects of endwalls and airfoils. Because the viscosity is the source of losses in turbomachines, its effect on fluid flow cannot be entirely neglected in the design of turbomachines. Generally at the beginning design of an axial flow turbine stages, various losses models and performance estimation are necessary. A number of methods of performance estimation have been published in the past, such as that of profile loss correlations [6] [7], shock loss model [8] and tip clearance loss model [9], etc. Some approximate engineering methods first suggested in [10] and [11] and now is developed and widely used in the present codes [12]. These methods make use of data from a large number of turbine tests and other associated test work reported elsewhere, providing an estimation of the flow parameters. However, such losses correlations should be reviewed and updated to make a better estimation of turbine performances. Ultimately it can be imagined that Three-Dimensional (3D) viscous calculations can be linked to blade design to give a complete definition of the flow field for turbomachines. Numerical simulated loss is incorporated into the design mode in which computation is used to obtain a required flow specification. Successful applications of the various inverse methods in the improvement of Two-Dimensional (2D) and 3D blading had been reported in references [13] and [14]. The results presented by Páscoa [15] showed a decrease in the losses and a better redistribution of the exit flow angle. Roidl and

Ghaly [16] redesigned a low speed turbine stage with a new inverse viscous design method, in this way the performance of the stage improved. However, those methods are only available for inverse problem, the direct problem still needs a simpler method that incorporates the most important aspects of the complex flow field, and can be used quickly and often in the design process.

This paper presents the VCV design of a 1.5 stage turbine. Particular emphasis is put on the design procedure and the flow field analysis with Computational Fluid Dynamics (CFD). The VCV design method is an approximate method first suggested in [17] by Gao and Zheng, which is an extension of CV design system. The method starts with the analysis of initial turbine geometry of a 1.5-stage turbine, then local numerical viscous losses are taken into account and the loss corrections are combined into the terms of the CV design equations to modify the CV design method. Reference [17] deals apparently with a low pressure turbine involving VCV design. This paper is a design practice based on VCV concept. It is a continuous work to provide sufficient information about how to control the vortex and combine the losses corrections effectively.

NOMENCLATURE

c	Absolute velocity [m/s]
G	Mass flow rate [kg/s]
B	Axial chord [mm]
C	Chord length [mm]
D	Diameter [mm]
h	Specific enthalpy [J/kg]
H	Average blade height [mm]
i	Incidence angle [°]
N	Number of blades [–]
n	Rotating speed [rpm]
o	Throat width [mm]
p	Static pressure [Pa]
r	Radius coordinate [m]
Re	Reynolds number [–]
T	Static temperature [K]
t	Pitch [mm]
u	Circumferential velocity [m/s]
y^+	Wall distance of first cell [–]
S1	Circumferential stream surface
S2m	Meridional stream surface

GREEKS

λ	Stagger angle [°]
α	Flow angle in absolute frame of reference (from tangential) [°]
β	Flow angle in relative frame of reference (from tangential) [°]
Ω	Stage reaction [–]
ζ	Total pressure loss coefficient [–]
η	Efficiency [–]
θ	Turning flow ange [°]
ρ	Density [kg/m^3]
w	Relative velocity [m/s]

SUBSCRIPTS

0, 1, 2	Guide vane inlet, Guide vane outlet, Rotor exit
is	Issentropic
m	Meridional component
u, r, z	Pitchwise, spanwise, streamwise directions
w	Relative thermodynamic parameters

SUPERSCRIPTS

*	Total thermodynamic parameters

ABBREVIATIONS

2D	Two-dimensional
3D	Three-dimensional
CFD	Computational Fluid Dynamics
CV	Controlled vortex
FV	Free vortex
GV	Guide vane
LE	Leading edge
NFV	Non-free vortex
PS	Pressure side
RANS	Reynolds-averaged Navier-Stokes equations
SS	Suction side
TE	Trailing edge
VCV	Viscous controlled vortex
VIGV	Variable Inlet Guide Vane

OVERVIEW OF THE 1.5-STAGE TURBINE

A 1.5-stage axial subsonic test turbine has been designed and built at Harbin Engineering University. The objectives of this test turbine to advance the understanding of complex flow phenomena in the turbine stage, to investigate the steady and unsteady aerodynamic behaviors of a low pressure turbine, but primarily to study rotor-stator interactions and its influences on stage performance.

Fig.1 shows a schematic diagram of the turbine test rig. The test facility is an open loop system that has the advantage of adjustable pressure and temperature level for various Mach and Reynolds number under different conditions. The turbine is a special horizontal arrangement and is connected through couplings to a compressor system that works as a brake to maintain the desired operating speed. High pressure air is provided by a separate electrically driven compressor station, and then fed into the turbine inlet casing via a special mixer insert, which is also fed by the hot compressed air from the brake compressor. The maximum mass flow is 17 kg/s with a pressure ratio up to 0.22 MPa in operation. Two water cooling heat exchangers are used to achieve elevated temperatures at test section inlet in order to maintain a constant temperature in the system. The compressed air temperature can be adjusted from about 420 K down to 300 K in the coolers.

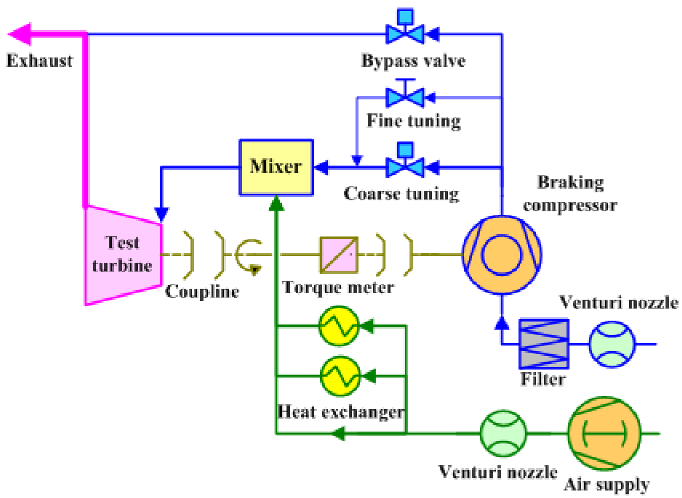

Fig.1 Schematic diagram of the turbine test rig

Some basic features of this turbine are summarized in Table 1. The objective of this paper is to use VCV design method to improve its adiabatic efficiency. Under the designed working conditions, the inlet Reynolds number and Mach number are 4.6e+05 and 0.21, respectively.

Table 1 Turbine Main features

Inlet total temperature (K)	402
Inlet total pressure (Pa)	220000
Outlet static pressure (Pa)	101300
Rotor speed (rpm)	7000
Mass flow (kg/s)	16
Blade height (mm)	80
Casing diameter (mm)	500
Hub diameter (mm)	340

The cross section of the 1.5-stage axial subsonic turbine is shown in Fig.2, with some of the main components highlighted. The turbine is comprised of an Inlet Guide Vane (IGV) row, one rotor row and a next stator row. Variable geometry built into the IGV component, which there is a rotational mechanical system that can turn 10 degrees angle in both directions. Each vane, rotor and stator cascades are made up of tapered and twisted blades. The flowpath is a cylinder flow channel due to the requirements of the straight optical windows and a cylindrical hub flow path for optical reflection capability. A cantilevered turbine rotor structure is used since this arrangement can open the space upstream the turbine for easy access during measurements and replacements. Additionally, the relative axial and circumferential positions of blade rows are adjustable because of the parallel, cylindrical hub and tip walls. The horizontal split plane of the whole facility (except diffuser inserts) provides ease of maintenance and rapid retrofit, which is further improved through the modular design of the test turbine. It seems that the test turbine is fully meeting the intended research application requirements attaining the advanced levels of the turbine design [18]-[23].

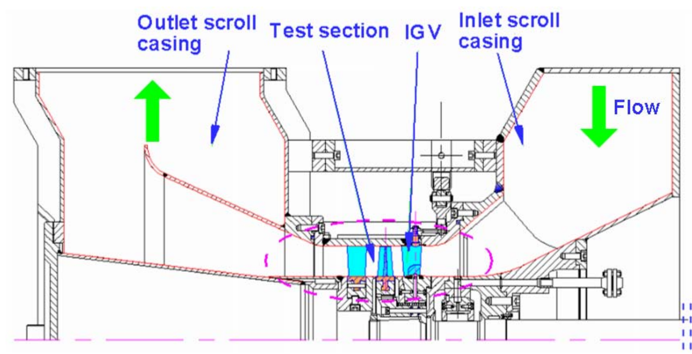

Fig.2 Cross section of the 1.5-stage turbine

In the present work, the approach similar to reference [17] proposed by Zheng et al was adopted, which consists in coupling CFD analyses in the whole design process. The final objective is represented by the improvement of efficiency and power output, with the same mass flow as the original turbine. At the same time, the following constraints are to be satisfied, which enable the direct fitting of the new geometry in the original turbine:

◇ The meridional flow-path unchanged;
◇ The blade axial chord unchanged, for both stators and rotors;
◇ The blade count of each blade row unchanged.

The design and optimization procedure is based on 3D Reynolds-Averaged Navier-Stokes equations solver.

DESIGN METHOD

In this section, a detailed description of the design and optimization procedure is provided, and the aerodynamic performances of the optimized turbine are discussed and compared to the original ones.

Controlled Vortex Design

The characteristics of test turbine are as followings:

◇ Additional stator blade row
◇ Parallel and cylinder flow channel for optical instrumentation
◇ Larger blade thickness due to the Variable Inlet Guide Vane (VIGV)
◇ Wider axial spacing between blade rows for experimental measurements
◇ Lower hub to tip ratio

Despite those restrictions, the CV design method was adopted for preliminary design to improve efficiency as far as possible.

In the present work, the radial-equilibrium equation for vaneless clearance is

$$\frac{1}{\rho}\frac{\partial p}{\partial r}=\frac{c_u^2}{r}+\frac{c_m^2}{r_m}\cos\delta-\frac{\sin\delta}{2}\frac{\partial c_m^2}{\partial m} \tag{1}$$

Note that the hub and tip walls are parallel and cylindrical, the meridional divergence angle δ would be equal to 0 degree and meridian radius of curvature r_{m} would tend to infinity. Equation (1) reduces to

$$\frac{1}{\rho}\frac{\partial p}{\partial r}=\frac{c_u^2}{r} \tag{2}$$

Substituting $h^{*}=h+c^2/2$ and $c^2=c_{\mathrm{u}}^2+c_{\mathrm{z}}^2$ into first law of thermodynamics

$$T\frac{\partial s}{\partial r}=\frac{\partial h}{\partial r}-\frac{1}{\rho}\frac{\partial p}{\partial r} \tag{3}$$

Combining equations (2) and (3)

$$\frac{\partial c_{\mathrm{z}}^2}{\partial r}=2\left(\frac{\partial h^{*}}{\partial r}-T\frac{\partial s}{\partial r}\right)-\frac{1}{r^2}\frac{\partial\left(c_{\mathrm{u}}r\right)^2}{\partial r} \tag{4}$$

The CV equation relating the meridional (axial) and circumferential velocity components, c_{z} and c_{u}, as functions of the radius r can be obtained and stated as follows

$$\frac{\mathrm{d}c_{\mathrm{z}}^2}{\mathrm{d}r}=2\left(\frac{\mathrm{d}h^{*}}{\mathrm{d}r}-T\frac{\mathrm{d}s}{\mathrm{d}r}\right)-\frac{1}{r^2}\frac{\mathrm{d}\left(c_{\mathrm{u}}r\right)^2}{\mathrm{d}r} \tag{5}$$

For the expansion process through a turbine blade, the entropy variation is small (ideally zero) compared to the variation in stagnation enthalpy across an exit port. Therefore, it may be assumed that $T\mathrm{d}s/\mathrm{d}r$ is much less than $\mathrm{d}h^{*}/\mathrm{d}r$. The $T\mathrm{d}s/\mathrm{d}r$ term is thus neglected.

Using the assumption of isenthalpic flow through the turbine vane and the definition of stagnation enthalpy, the equation (5) may be simplified to

$$\frac{\mathrm{d}c_{\mathrm{z}}^2}{\mathrm{d}r}=-\frac{1}{r^2}\frac{\mathrm{d}\left(c_{\mathrm{u}}r\right)^2}{\mathrm{d}r} \tag{6}$$

Approximately, we assume that the stage enthalpy drop is constant with respect to the radius. In this study, equation (6) is still applicable at the turbine stage exit.

The assumption of axial velocity at fixed radius allows equation (6) to be solved for tangential velocity. This indicates that with different distributions of $c_{\mathrm{u}}(r)$ and $c_{\mathrm{z}}(r)$, we will obtain different design results. The so-called optimal flow-type problem is to select one set of distributions that evolve optimal results. This question has moved from solving circulation distribution to solving axial velocity.

In tradition, the flow variations in the spanwise direction at a span calculation station can be taken into account by supplying the streamtube as a function of the meridional coordinate, and usually obtained with one-dimensional meridional analysis. For the CV design, however, this type of assumption on the streamtube is unsatisfactory because substantial spanwise flow components present in the flow field as shown in Fig.3. This Q3D assumption is especially invalid near the end regions of a blade, where 3D effects are strong. The applications of sectional design methods using Q3D flow physics are thus confined to mid-span regions.

In CV design, the flow angles relative to the tangential direction have been decreased at guide vane (GV) exit and increased at rotor exit in the radial direction to shift flow radially inward. Those make the blades negative twisted meanwhile. The strong contraction streamlines in stream-wise direction cause an opposing centrifugal force to offset the radial pressure gradient. The lower pressure gradient produces a "flat" reaction gradient over the blade height. This is the evidence of controlling the reaction gradient.

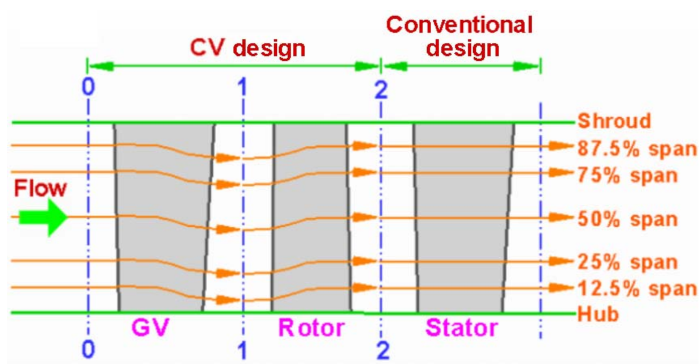

Fig.3 The streamline distortions in CV design turbine

The decreased flow angle α_1 at vane outlet and increased flow angle β_2 at rotor outlet are inclined to induce the radial blade forces, as shown in Fig.4 (a). The effects are almost confined in the rear part of stator and the front part of rotor, which have little influence upstream and downstream of turbine stage as illustrated in Fig.4 (b). The static pressure is reduced at the tip and increased at the hub in the CV design turbine stage. These effects produce a significant influence in the tip and hub regions, so that its streamlines face inwards. The reaction at the root is increased in varying degrees to improve rotor performance, and tip reaction is generally decreased relative to a FV design to reduce tip leakage. This technique applied to design a turbine stage that biases the flow toward the more efficient area and secure positive hub reaction.

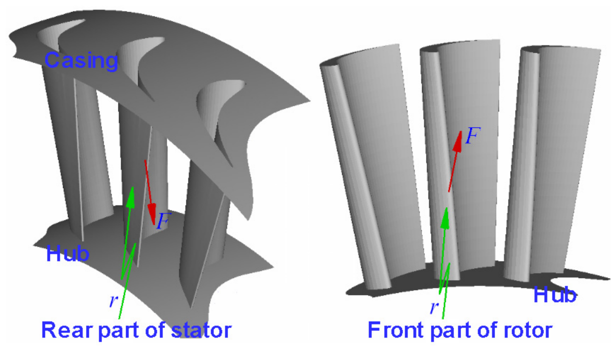

(a) blade negative twist

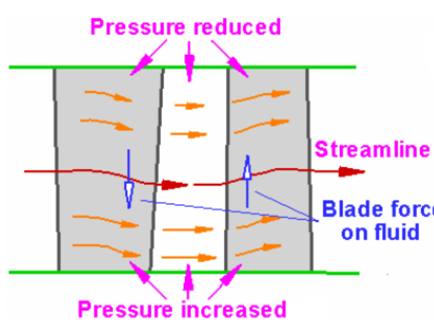

(b) the effect

Fig.4 The effect of blade negative twist

Traditional design method assumes that the stream surfaces remain cylindrical along the blade rows. Differential form of continuity equation can be written as

$$\partial(\rho A c_z)/\partial z=0 \tag{7}$$

Thus, representing the elementary mass flowrate by $\rho A c_z$, the elementary continuity equation is obtained. Typically, the first turbine stage is designed for zero inlet swirl (α_0=0), so equation (7) can be written as

$$\rho A c_z=\rho_0 A_0 c_0 \tag{8}$$

It is possible to show that radial deviations of the stream surfaces associated with changes in meridional (axial) velocity are indeed negligible in traditional design situations. However, in CV design the stream surfaces are distorted towards the hub sections, the cylindrical stream surfaces no longer exist. A new method would be in quest for to deal with the stream surface distortions.

As described in Fig.4, we could introduce the assumption that the fluid radial migration and the radial velocity are only in blade rows. The radial velocity is tiny and can be neglected at the rotor-stator interfaces. So it could organize the flow at the rotor-stator interfaces by means of different axial flow velocity distributions. The axial velocity between the rows is also determined by the inlet velocity according to equation (8). Once the inlet flow velocity is given, other interface axial velocities could be resolved uniquely through equation (8). Hence the equation (8) can still be used in CV design. The first step in the analysis was to determine the best axial velocity profile. The free vortex distribution was immediately ruled out since it provides constant work along the blade height. The constant mass flow distribution was also investigated, but the mass flow then increased above the required 16 kg/s, then we had to turn the vane somewhat closer to get some lower reaction at the tip. This can be termed as conventional design. Then we turn the vane further closer at the tip and somewhat open at the hub to obtain the CV design. The different inlet flow velocity distributions are shown in Fig.5. The inlet velocity distribution used in conventional design stage is the red line marked with square symbols, the green line marked with a delta symbol is the inlet velocity distribution used in CV design stage. For comparison, the inlet velocity distribution of the constant massflow design is also given in the Fig.5. The axial velocity diagram represents the symbolic massflow distribution in spanwise. In Fig.5, the massflow is slightly higher at the hub than the tip in CV design stage. Even so the inlet velocity mentioned in this paper is pseudo and not the real flow situation. We introduced the inlet velocity just in order to control the flow in CV design stage.

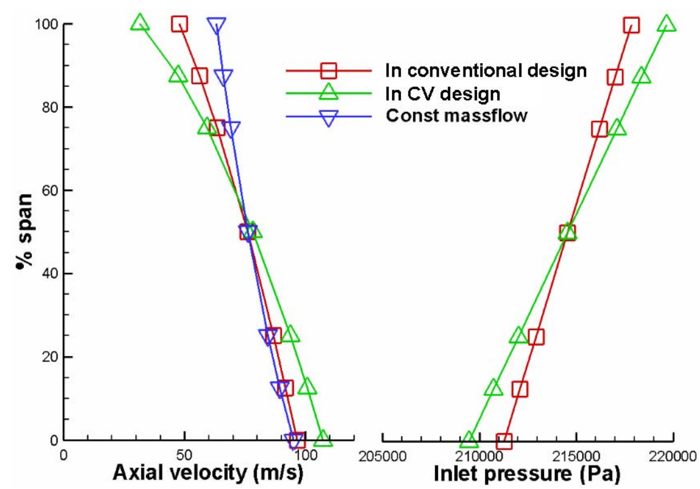

Fig.5 The inlet velocity and pressure

The effects of velocity variations can be simply illustrated by the velocity triangles in Fig.6. This figure shows two different radial positions, namely near the tip and near the hub as illustrated. The axial velocity has increased at the root and decreased at the tip to shift flow radially inward toward the root comparing to the conventional design. Obviously, this guarantees that the global massflow would be same.

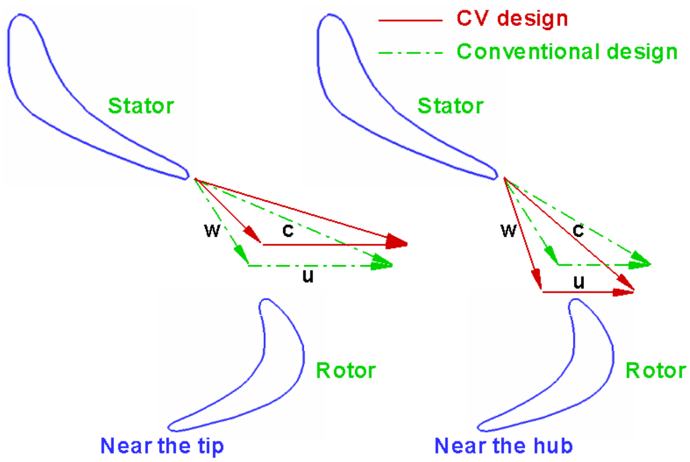

Fig.6 The velocity triangles at different radial positions

Based on equation (8), the massflow could be a function of the pressure distribution

$$\rho A c_z = \rho_0 A_0 c_0 = f(p) \quad (9)$$

So the pressure distribution was specified instead of circulation to resolve the axial velocity distribution. The choice of substituted pressure distribution contributes to the following several reasons: (1) The specified pressure distribution has the minimal deviations due to its magnitude while the velocity distribution is sensitive to the boundary layer; (2) The pressure distribution can more easily satisfy the requirements of radial equilibrium inside a turbine stage; (3) The pressure distribution tends to simple curves like straight line while the circulation appears to high-order polynomial cures. The two different inlet pressure distributions specified in this study are shown in Fig.5, other blade exit pressure distributions can be seen from Fig.10 (with red lines marked with square symbols). For simplicity, the pressure distributions at all computational stations are linear. The pressure distribution at mean radius and other radius were chosen based on good choices of reaction, work coefficient and flow coefficient.

The whole solution procedure is illustrated in Fig.7. As can be seen from the diagram, the circulation distribution is not directly given. The final flow angle is a joint decision of axial velocity c_z distribution and pressure p distribution.

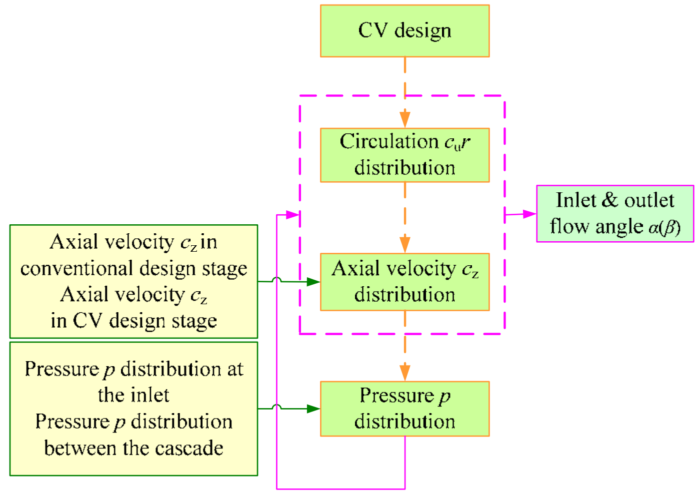

Fig.7 The solution procedure

The GV, rotor and stator were designed in five streamline sections corresponding roughly to 12.5, 25, 50, 75 and 87.5% of the annulus height. The design technique consists of the following: (a) definition of the geometry of each airfoil section, (b) stacking the blade and checking that all geometric parameters varied smoothly over the airfoil height, (c) running multi-stage numerical solution for design turbine, (d) making adjustments to geometry where is necessary and repeating the cycle if necessary until achieving a satisfactory turbine design.

VCV design and optimization approach

The current VCV method consists of three integrated parts to determine the required geometrical modification to accomplish the final target of increasing efficiency. The first is the flow analysis, the second is the loss correction, and the third is the blade modification. The design process starts with analysis of the CV design blades by means of high fidelity CFD simulations. The basic steps in VCV design procedure are given in Fig.8. What VCV design offers in this system is an analytical tool that allows the designer to achieve the design intent. The VCV design method would be used to guide the modification in blade geometry, when multistage analysis indicates a significant local incidence mismatch. More details are given below to illustrate this design process.

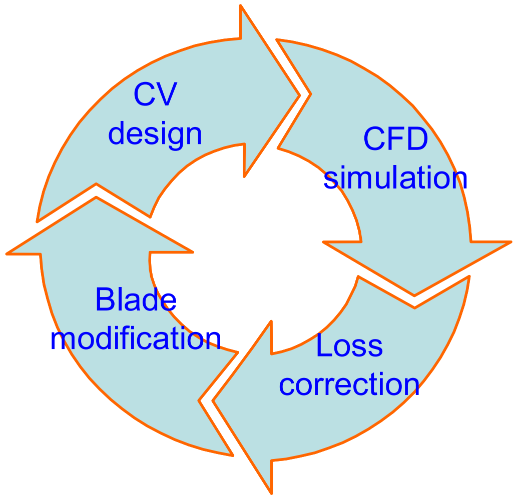

Fig.8 VCV design and optimization loop

The real, 3D, viscous effects of secondary flow, overtip leakage, etc. and their subsequent mixing with what may be termed as the primary flow, have not been considered in terms of local features in CV design. It should be emphasized that the precise design procedure must take into account the 3D nature of the flow and also the effects of the fluid viscosity. Hence, a method of loss component estimation along radius is a subject of importance.

In recent years, a great interest has been focused on the use of CFD for the optimization of modern gas turbine engines. This is to be seen as a major opportunity to upgrade traditional design system and to develop the next generation of modeling capabilities in order to offer performance improvements over and above what can currently be achieved. Ultimately it can be imagined that the flow losses and deviations are completely assessed by using CFD calculations. The code used here is EURANUS from Numeca, the numerical method would be introduced in the reference.

The VCV method began with the analysis of initial turbine geometry, the CV design method was modified to take the local viscous losses into account. The increase in entropy is used to take account of the effects of viscosity and other losses, e.g., separation of boundary layer, leakage flow, etc. The first step is the entropy corrections to equation (5). The circumferentially mass averaged entropy value in the radial direction is estimated from CFD value. In essence, this approximate model means that only the accumulated effects of upstream viscous actions in increasing the entropy are considered in the flow calculation. The comparisons between corrected entropy distribution and isentropic distribution at blade exit can be seen from Fig.9. The deviations are observed near the endwalls.

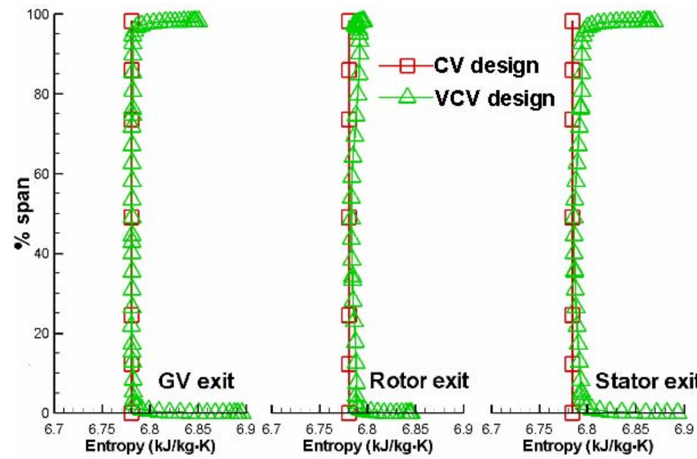

Fig.9 Entropy corrections

The second step is the pressure corrections to equation (3). The pressure value in equation (3) is also refined from CFD to reduce the deviation between throughflow analysis results and CV design results, see Fig.10. The minimal deviation from the static pressure between the initial design and the final design confirms that the approach giving pressure distribution to resolve circulation distribution is effective and reliable. After those corrections, the term static enthalpy is changed accordingly, other parameters such as axial velocity and tangential velocity is also changed simultaneously. By the way, the design equilibrium is restored amongst blading work capacity (linked to radial pressure distribution) and entropy production, providing an efficient means for tailoring blade shapes.

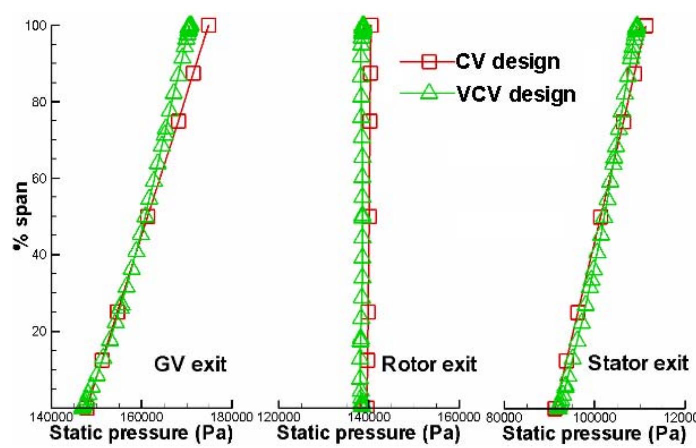

Fig.10 Pressure corrections

The corresponding changes of flow angles are shown in Fig.11. A comparison is made between the CV design method described as the original design and the results obtained with the application of VCV. The flow angles along the radius at each station are determined by an iterative solution. As shown in Fig.11, the exit flow angle was altered as little as possible from the CV design. In this study it was found that the entropy corrections and pressure refinement have little effect on the Trailing Edge (TE) angles onto the next blade. The rotor inlet flow angle β_1 is reduced from about 65° to roughly 45° at the tip and decreased almost the upper part. It can be seen that the VCV design gives an approach to reduce the inlet rotor flow angle β_1 by unloading the rotor tip. The VCV design also offers a potential to avoid highly twisted blades, for simplicity in manufacturing. The latter changed result in stator is slightly more twisted, which does not significantly change the radial distribution of absolute swirl angle at rotor exit.

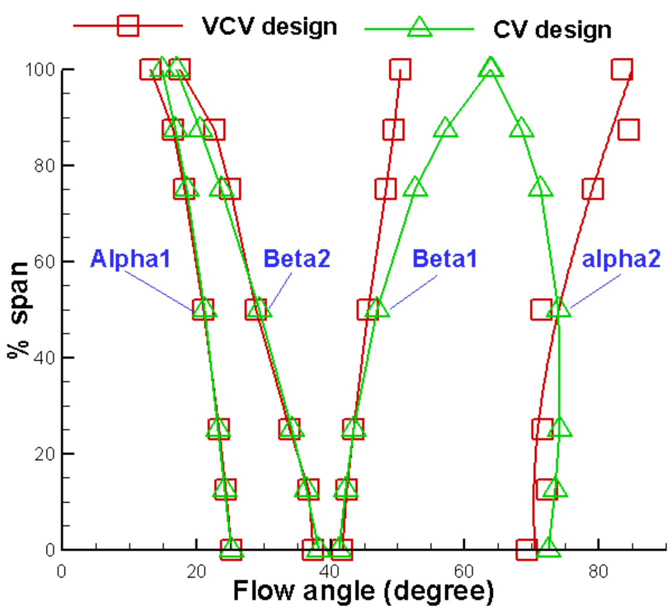

Fig.11 variations of flow angles for various flow patterns

The effects of entropy corrections and pressure refinements can be simply illustrated through the use of velocity triangles in Fig.12. In Fig.12, the GV exit angle α_1 is decreased, so the stagger angle λ has to increase to some degree. The stagger angle λ in the tip section is adjusted appropriately to guarantee massflow and keep the same the passage throat widths. High velocity jets are induced at the vane exit, leading to high positive incidence downstream of the GV. As a consequence, the relative flow angle at the rotor inlet was modified. Additionally, the Fig.12 also demonstrates the abrupt changes in velocity magnitude near the TE of upstream rotor in dot dashed lines.

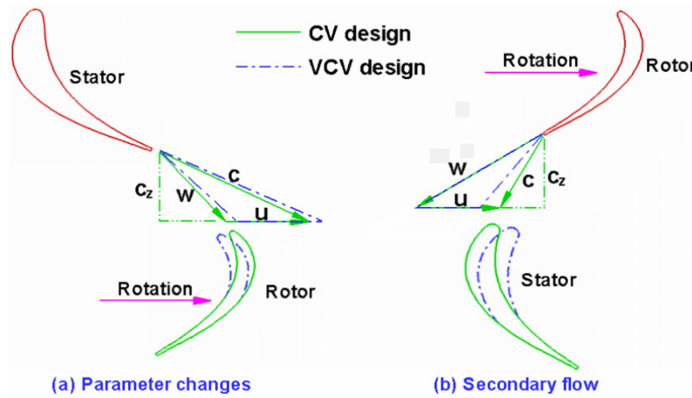

Fig.12 The blade changes due to the parameter changes

In reality, the profile loss, secondary loss, and leakage loss are the main factors of stage match or stage mismatch. The Fig.13 shows that the fluid from the upstream airfoil wake will migrate towards the Suction Side (SS) of the downstream airfoil, leading to a large negative incidence angle at the Leading Edge (LE) of downstream blade row. The flow leaking over the tip clearance reenters the main flow path on the downstream side of the rotor with a high tangential velocity component. The still largely tangential flow must mix with the largely axial flow leaving the rotor. This generates mixing losses and can lead to incidence angle problems in the downstream stator. The impact of leakage is the same to the secondary flow. Typically the tip leakage loss accounts for almost 1/3 of the overall turbine stage losses. This is the reason why there is a bigger change to the stator inlet flow angle at the tip than that at the root. Due to this rotor deviation, the resulting inlet flow angle into the stator changes by something more than 20 degrees as can be seen in the Fig.11.

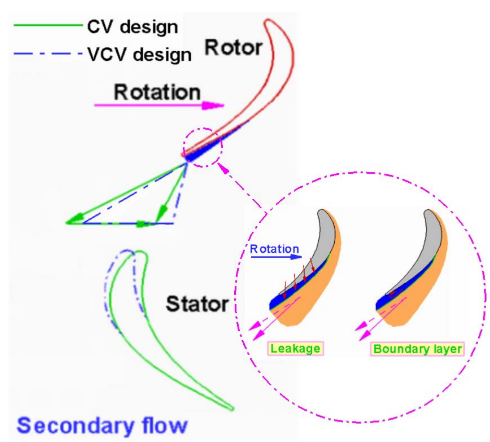

Fig.13 The stator changes due to the secondary flow

Fig.14 illustrates the changes of all blade geometries in three radial sections. The choices of LE inclination are influenced by the "induced incidence" produced as a result of losses and deviations. The exit angle was altered as little as possible from the CV stage. 3D view of the initial and optimized geometries of rotor is also shown in Fig.14. Main differences concern the LE region of the upper part of the blade, which is characterized by a higher surface curvature.

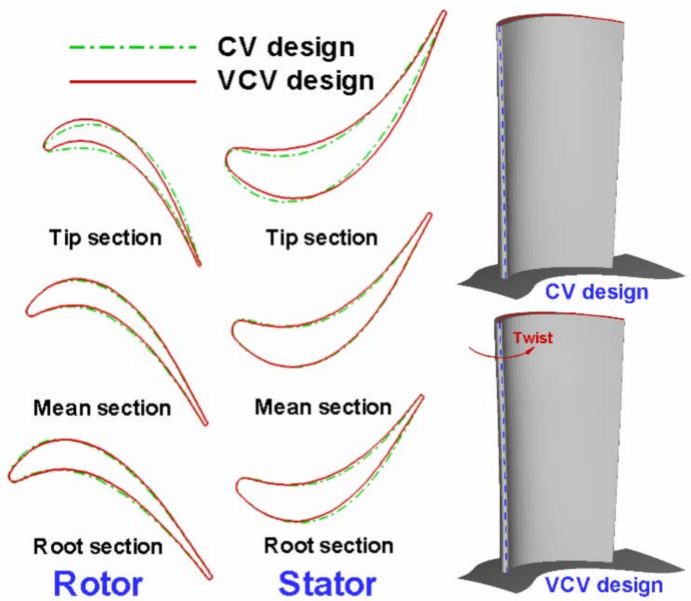

Fig.14 Blade sections for VCV design versus CV design

The final 3D turbine model is shown in Fig.15. The vanes and stators were stacked at LE, the rotor blades were stacked at the centerline of gravity. There are 30 variable inlet guide vanes and 45 rotor blades followed by 32 stator blades. The final blade geometries look very smooth.

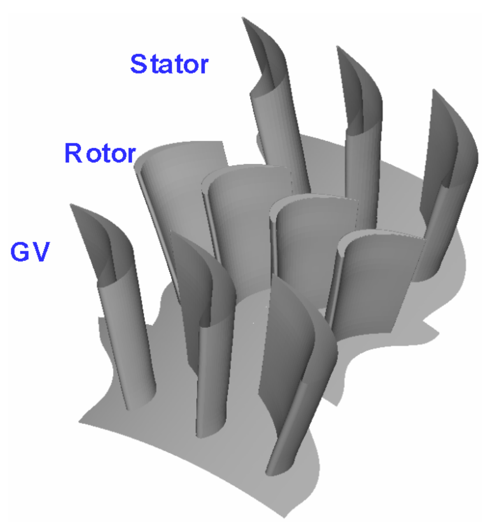

Fig.15 3D turbine geometry

COMPUTATIONAL PROCEDURE

After the blades are designed, a 3D viscous code is used to verify the design and the results can provide more information about the flows.

Flow Solver

Flow solutions were obtained by EURANUS from Numeca. The solving method is a cell-centered finite volume scheme of Jameson type to solve the RANS equations with second-order artificial viscosity. The time integration was performed using an explicit, four-stage Runge-Kutta scheme. To speed up convergence to steady state, local time stepping, implicit residual smoothing and multi-grid acceleration techniques were applied. A One-equation Spalart-Allmaras turbulence model was chosen for the turbulence closure. The conservative coupling by pitchwise row approach had been adopted to model the rotor-stator interaction problem for steady flow analysis. The EURANUS solver had been parallelized using the domain decomposition method and run efficiently on both shared and distributed memory computers.

Typical computations required approximately 1000 iterations. The solutions were considered converged when the scaled residuals of all equations were resolved to levels of order of magnitude of 10^{-6}.

Computation grid

The computational domains of CV design and VCV design were discretized by IGG/AutoGrid with transfinite interpolation and elliptic grid generator. Structured multi-block grids were generated. Fig.16 (a) shows the multi-block structured grids around the blades in the complete numerical domain. H-type grids for the inlet and outlet flow region, O4H-type grids (Four H-type grids for external blocks and an O mesh for internal block) around the blades rows, and O-type grids for tip-clearance region, were involved. The orthogonal body-fitted O mesh was employed to reduce grid skewness and to capture the viscous region in the vicinity of the aerofoil whilst four H meshes are adopted near the periodic boundaries, upstream and downstream blocks.

Fig.16 (b) shows a detail of the mesh topology in the tip clearance region with close-ups around LE and TE. The mesh refinements were adapted in blade surface and wall boundary layers, around leading and trailing edge planes and in wake of each blade row. On the periodic boundaries, the nodes are not coincident, but lie on the same surface for an accurate interpolation. More information about the IGG/Autogrid mesh generator could refer to [24].

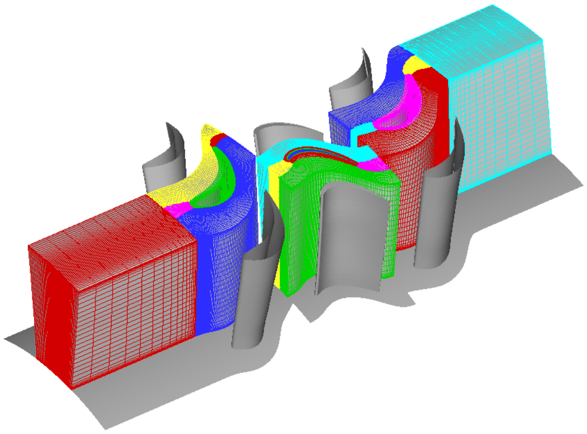

(a) Computation domain

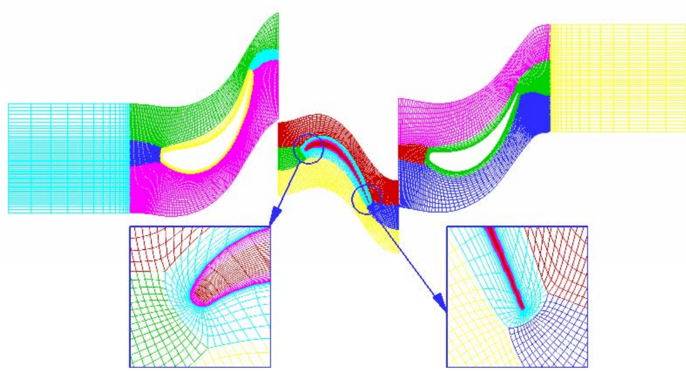

(b) Blade-to-blade mesh

Fig.16 Computation domain and B2B mesh

The computational grids consist of 57×17×57 (blade-to-blade, axial, spanwise) H-type grids at inlet and 41×17×57 outlet, 57×101×57 O4H-type grids around GV, 41×85×57 rotor including 9 radial cell layers for the tip clearance and 41×105×57 stator. The full grid results of CV design and VCV design keep the same level, in a total mesh size of around 1.2e+06 nodes respectively, further refinement was found to be unnecessary for the fidelity of the numerical solution. The first grip point off the solid surface is typically placed at a y^+ value of 1.0.

The total pressure, total temperature and flow angle were fixed at the inflow boundary, while the average static-pressure was imposed at the outflow. Periodic boundary conditions were applied on the lateral faces of the flow domain. The walls were treated as adiabatic and a no-slip condition was enforced. An angular velocity corresponding to the nominal rotational-speed of turbine was applied.

DESIGN RESULT ANALYSIS

Outputs of CFD calculations used for turbomachinery analysis can be put into two main categories: 1) Integral flow performances (mass flow rate, power and the efficiency); 2) Detail flow characteristics (distributions of loss coefficient, velocities, pressures and so on the control stations, namely inlet, between blades and outlet.

Integral flow performances

In Table 2 we summarize the global computed performance results. In this section, the VCV design method is applied to the 1.5-stage axial turbine and the results are compared with the CV design. A global performance gain is confirmed using VCV design method. The configuration implies 0.2% improvement of stage efficiency relative to the base geometry. The massflow and total pressure ratio maintain the same level as the CV design. Other properties such as power and torque are also increased.

Table 2 Computational results

	CV design	VCV design	Increment (%)
Massflow (kg/s)	16.13	16.1	-0.19
Efficiency (%)	89.55	89.75	0.2
Pressure Ratio (-)	0.65845	0.65722	-0.19
Power (kW)	657.53	663.64	0.93
Torque (N·m)	897	905.33	0.93

Detail flow characteristics

1. Streamline distributions at 90% span

In the design process of gas turbine cascades, attentions must be paid to the differences between flow angles and blade metal angles. To this point, all of the calculations pertaining to the flow angles are required to achieve the design specifications. Considerations must be made for the incidence and deviation occurred at the blade LE or TE, respectively.

According to the Fig.14, the main differences occur in the upper part of the span height, from midspan to the blade tip. Fig.17 shows the calculated streamlines and the relative velocity contour at 90% blade height. These results are derived from the CFD simulation. Typically, the GV is designed for zero inlet swirl (α_0=0), and there is free of separation phenomenon in the main flow. A high positive incidence is observed at the LE of rotor and a negative incidence at the LE of stator respectively in the CV design, as expected. The results also indicate that the incidence is close to zero after entropy corrections and pressure refinements.

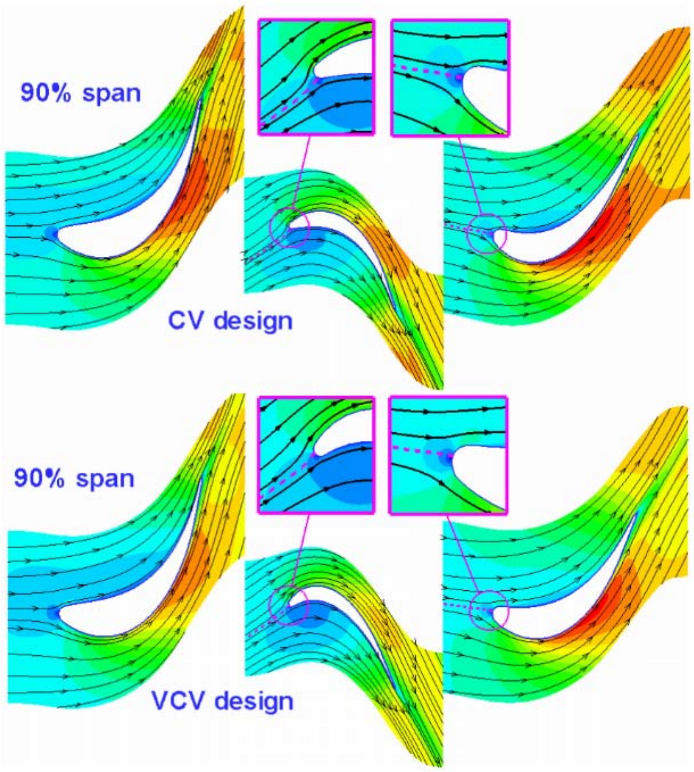

Fig.17 Streamline distribution at 90% span

2. Loss coefficient along the blade height

The total pressure loss coefficients for the stator and rotor are defined as followings:

$$\bar{\omega}_1 = \frac{p_0^* - p_1^*}{p_1^* - p_1} \qquad \text{For stator} \tag{10}$$

$$\bar{\omega}_2 = \frac{p_{w1}^* - p_{w2}^*}{p_{w2}^* - p_2} \qquad \text{For rotor} \tag{11}$$

The effects of upstream blade onto downstream blade could be eliminated by using these equations instead of radial efficiency distributions.

The radial variations of total pressure loss coefficient at the blade exit are given in Fig.16. The loss coefficient is the circumferentially mass averaged data. The red lines marked with square symbols represent the results of VCV design, whereas the green lines with delta symbols are associated to CV design. The improvement occurs in the outer part of the rotor (95% span), as shown by the large reduction of total pressure loss coefficient in the tip section. The figure also illustrates that the spanwise distributions of the total pressure loss coefficient in GV and stator are similar for various design methods. A large portion of blade row inefficiency can be attributed to the pressure loss occurring near the rotor endwalls.

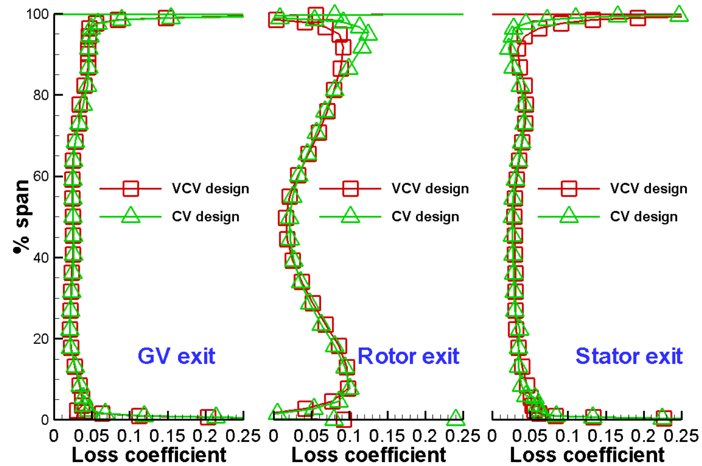

Fig.18 Spanwise loss coefficient for CV and VCV designs

3. Pressure distributions along the blade surface

Fig.19 presents the static pressure distributions in three sections along the blade span, at hub, mid section and tip. The VCV design produces changes in the pressure distributions along the blade height, but the overall load is nearly the same at the different radial locations. For GV as shown in Fig.19 (a), the loading increases a little bit, but essentially remains unchanged. The numerical flow simulation shows that the flow is well behaved on the blade Pressure Side (PS), only a small diffusion region is on the SS between 65% chord and the TE, where the flow may behave rather poorly. For stator shown in Fig.19 (b), the differences are very distinct near the hub. The hub is intent to unload in VCV design with the purpose of energizing the hub boundary layer in order to prevent separation there. Additionally, the GV and rotor are typically aft-load blades which could efficiently delay the boundary layer transition and enhance the turbine variable condition properties.

The static pressure distributions along the stator surface are shown in Fig.19 (c). The load is pushed slightly backward at the tip, and the rotor has better incidence characteristics in the upper part of the blade. Static pressure at the LE of the SS increases after VCV design, as is evident from Fig.19 (c). The overshoot observed at LE in the lower part of the blade indicates that the fore-loaded configuration always comes with high incidence, which increases the amount work performed in the first 20% of the blade and reduces the pressure loading in the rest of the blade. Accordingly, the blade hub section is expected to reduce the LE loading to initiate less secondary flow.

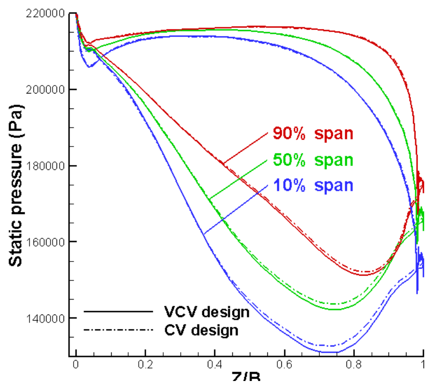

(a) GV blade

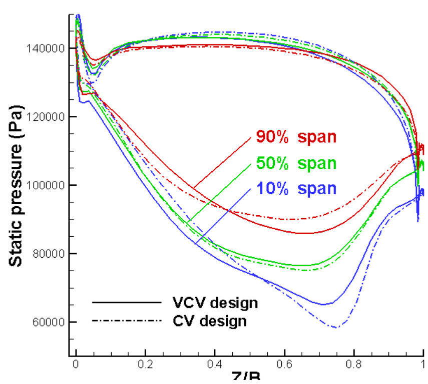

(b) Stator blade

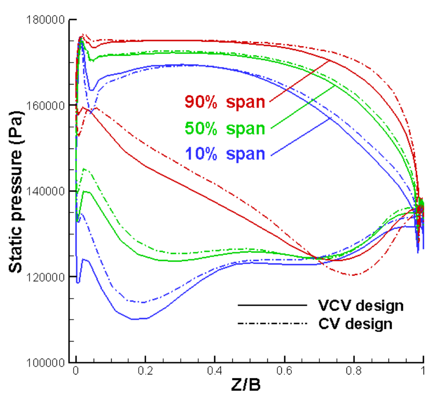

(c) Rotor blade

Fig.19 Pressure distributions along the blade surface

4. Limiting streamline on the blade surface

To understand the vortex and loss transport mechanisms, the calculated limiting streamlines and the entropy contours on the suction surfaces are shown in Fig.20. For simplicity, the similar results will not be listed one by one, only the differences are expounded. As shown in Fig.20 (a) and (b), the features of the blade row surface flow are identical for GV and stator. The secondary flow boundary layer forms across the hub passage wall towards the suction surface and rolls upward on the suction surface, which is seen by the oblique streamlines in the rear-root corner region. While at the tip, a down press of the passage vortex is observed. As shown in Fig.20 (c), the streamlines show that there is a well established two-dimensional flow between 30% and 70% on the rotor surface. At the hub, a lift-off of the passage vortex is observed, while at the tip, larger differences can be seen in the secondary flow structures. The tip passage vortex appears quite complicated, because the leakage flow and the flow structures generated over the upper height of the blade in the rotor derive the loss production mechanisms. Comparing the top and below figures (see the PS leg of the horseshoe vortex), it can be concluded that a stronger transverse pressure gradient leads to a stronger uplift or down press of the passage vortex separation line on the rotor suction surface which increases the endwall low energy fluid migration along the blade surface. These behaviors can entrain the low-energy fluid into the main stream and reduce the secondary flow loss in both tip and hub regions, increasing the endwall work capability and restraining separation.

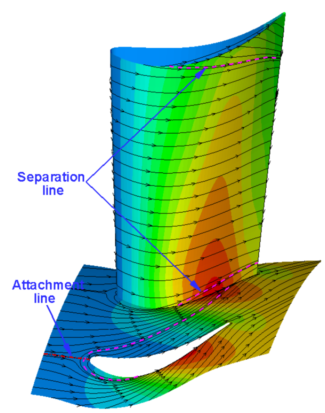

(a) GV blade surface

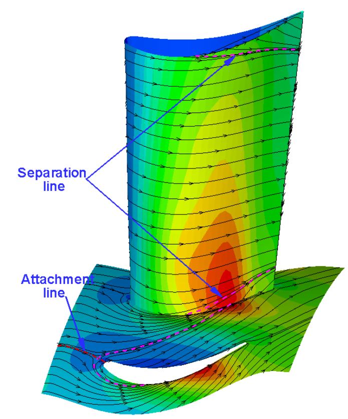

(b) Stator blade surface

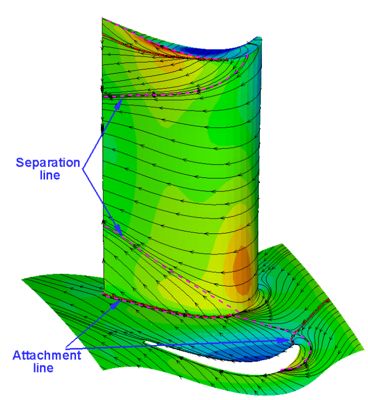

(c) Rotor blade surface

Fig.20 Limiting streamline for VCV design and CV design

Flow patterns on the rotor SS as shown in Fig.21, which indicate the convergence of streamlines. The overall effect of incidence is not really big to the passage vortex because the limiting streamline pattern of VCV design is the same as CV design. The main difference is circled out with a blue dashed line in the rear-tip corner region, as a consequence of the mixing of tip clearance leak flow and passage vortex with the mainstream. It should be noted that the performance improvement at rotor outlet is confined to the region near the tip because of the weak interactions between leakage flow and passage vortex. This is achieved by a backward blade loading and higher flow turning in VCV design at the tip, and therefore leakage loss is reduced.

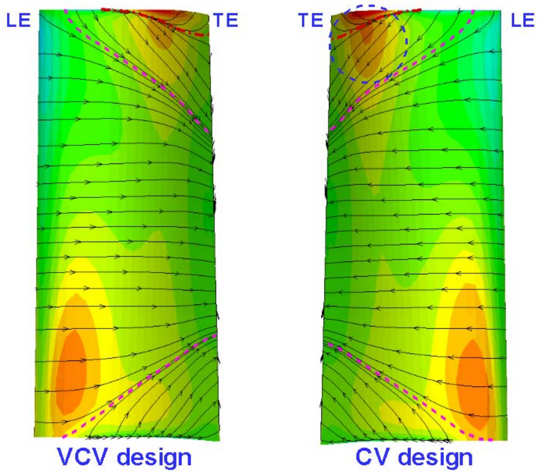

Fig.21 Flow patterns on rotor SS

5. Entropy distributions at the blade exit

The vanes exit entropy contours of GV and stator for the VCV design method are plotted in Fig.22. The left plot represents the GV exit, the right represents the stator. As shown in Fig.22, the most total losses of the vane come from the suction surface boundary layer, the passage vortex areas near the SS hub and tip. From the Fig.22, the great losses generated in the rotor reenter in the downstream stator and significantly affect the flow field of downstream stator. The result of this dynamic process is evident by a higher entropy value at the stator exit.

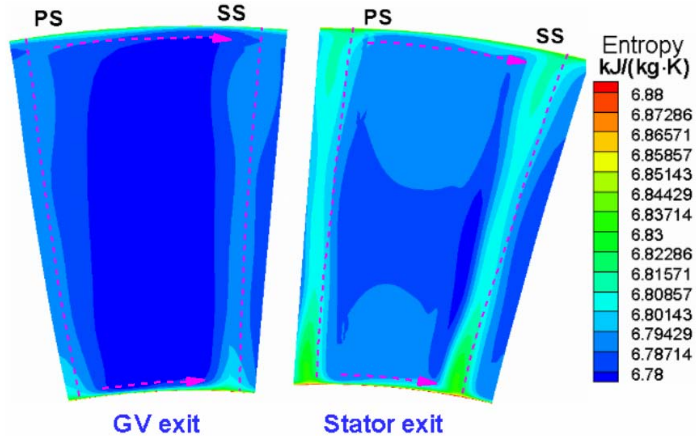

Fig.22 Entropy contours for VCV design

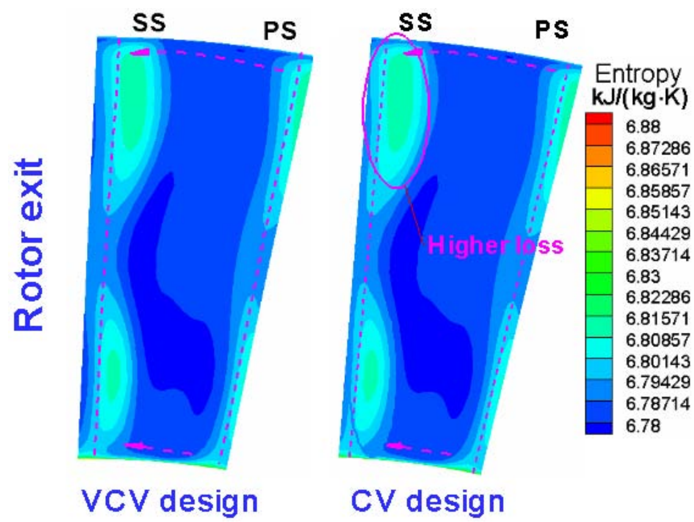

Fig.23 Comparison VCV design with CV design

In Fig.23 the radial distributions of the entropy at the rotor outlet plane are reported, two endwall zone high loss regions appear near the SS. The upper zone is larger than the lower as a consequence of the mixing of tip clearance leakage and vortex with the passage mainstream. The passage vortex experiences a strong transverse pressure gradient, entraining low momentum fluid away from the endwalls towards the midspan. Although the losses are reduced near the endwalls, it would increase in the mainstream. It is of importance to note that the passage vortex in turbine passages appears to be of no sufficient strength to make the two endwall zone loss regions merge into a single one. This also shows an improvement of stage efficiency in the region between around 70 to 100% of blade height in VCV design.

CONCLUSION

The conclusions of the researches and analyses in this paper can be summarized as followings:

1) The VCV design method is based on the CV design method to retain short computational time, which is an extension of the conventional inviscid throughflow approach. The VCV design method can take the real, 3D, viscous effects of secondary flow, overtip leakage, etc. and their subsequent mixing with the primary flow into account

2) The researches show that the VCV design method can improve stage matching through the loss corrections combined into the terms of the CV design. Compared with the traditional empirical correction and experiment calibration, the VCV design method is more quick and easy to incorporate CFD into blade design.

3) The design method demonstrates its ability to design blade rows that could improve efficiency near the endwalls. As a result of the entropy corrections and the pressure refinements, the adiabatic efficiency is successfully increased by 0.2%. Although the stream surfaces are distorted, extra mixing losses do not seem to be generated in or behind CV design stage.

4) It is likely that the numerical turbine performance can be attributed to the reduction of secondary flow losses in rotors, as shown in Fig.18, Fig.19 (c), Fig.20 (c) and Fig.23. These losses are large and may be reduced by adjusting primary structure features (e.g. blade aspect ratio, camber line, etc.) and secondary structure features (e.g. lean, bow, etc.) in order to reduce the secondary flow losses.

5) According to the results, the loading at the rotor tip is tend to be more uniform in favor of reducing leakage in the tip region. While at the rotor hub, a fore-loaded configuration at the rotor hub leads to a stronger transverse pressure gradient which makes the boundary layer thicken.

ACKNOWLEDGEMENT

The author would like to thank the many colleagues who helped undertake this research at College of Power and Energy Engineering, Harbin engineering university. The authors would like to acknowledge the support of China Doctoral Grant No. 20092304110004.

REFERENCE

[1] Vad, J., Bencze, F., Benigni, H., Glas, W. and Jaberg, H., 2002, “Comparative Investigation on Axial Flow Pump Rotors of Free Vortex and Non-Free Vortex Design”, Periodica Polytechnica Ser. Mech. Eng. Vol. 46, No. 2, pp.107–116

[2] Vad, J. and Bencze, F., 1998, “Three-dimensional flow in axial flow fans of non-free vortex design, Int. J. Heat and Fluid Flow”, Int. J. of Heat and Fluid Flow, Vol. 19, No. 6, pp. 601-607

[3] Szlivka F. and Molnár, I., 2008, “Measured and non-free vortex design results of axial flow fans”, J. Mechanical Science and Technology, Vol. 22, No. 10, pp. 1902-1907

[4] Albuquerque, R. B. F., Manzanares-Filho, N. and Oliveira, W., 2007, “Conceptual Optimization Of Axial-Flow Hydraulic Turbines With Non-Free Vortex Design”, Proc. IMechE, Part A: J. Power and Energy, Vol. 221, No. 5, pp: 713-725

[5] Plaia, J. M. and Lear, W. E., 1997, “Preliminary turbine design for non-uniform inlet conditions”, AIAA Paper No. AIAA-1997-3010

[6] König, W. M., Hennecke, D. K. and Fottner, L., 1996, “Improved Blade Profile Loss and Deviation Angle Models for Advanced Transonic Compressor Bladings: Part I—A Model for Subsonic Flow”, J. Turbomach., Vol. 118, No. 1, pp. 73-80

[7] König, W. M., Hennecke, D. K. and Fottner, L., 1996, “Improved Blade Profile Loss and Deviation Angle Models for Advanced Transonic Compressor Bladings: Part II—A Model for Supersonic Flow”, J. Turbomach., Vol. 118, No. 1, pp. 81-87

[8] Puterbaugh, S. L. and Copenhaver, W. W., 1997, “A Three-Dimensional Shock Loss Model Applied to an Aft-Swept, Transonic Compressor Rotor”, J. Turbomach., Vol. 119, No. 3, pp. 452-459

[9] Storer, J. A. and Cumpsty, N. A., 1994, “An Approximate Analysis and Prediction Method for Tip Clearance Loss in Axial Compressors”, J. Turbomach., Vol. 116, No.4, pp. 648-656

[10] Ainley, D. G. and Mathieson, G. C. R., 1951, “A Method of Performance Estimation for Axial-Flow Turbines”, Aeronautical Research Council, No. ARC-R/M-2974

[11] Craig, H. R. M., and Cox, H. J. A., 1970, “Performance estimation of axial flow turbines”, Proc. IMechE, Vol. 185, No. 32, pp. 407-424

[12] Kacker, S. C., Okapuu, U., 1982, “A Mean Line Prediction Method For Axial Flow Turbine Efficiency”, J. Engineering for Power, Vol. 104 No. 1, pp 111-119

[13] De Vito, L., Den Braembussche, R. A. V. and Deconinck, H., 2002, “A Novel Two Dimensional Viscous Inverse Design Method for Turbomachinery Blading”, ASME Paper No. GT-2002-30617

[14] Tiow, W. T. and Zangeneh, M., 2000, “A Three Dimensional Viscous Transonic Inverse Design Method”, ASME Paper No. 2000-GT-0525

[15] Páscoa, J. C., Mendes, A. C., and Gato, L. M. C., 2008, “Redesigning Annular Turbine Blade Rows Using a Viscous-Inviscid Inverse Design Method”, ASME Paper No. GT2008-50313

[16] Roidl, B. and Ghaly, W., 2008, “Redesign of a Low Speed Turbine Stage Using a New Viscous Inverse Design Method”, ASME Paper No. GT2008-51468

[17] Zheng, Q., Gao, J. and Li, B., 2010, “Study of Viscous Controlled Vortex Design of a LP Turbine Stage”, ASME Paper No. GT2010-23123

[18] Erhard, J. and Gehrer, A., 2000, “Design and Construction of a Transonic Test-Turbine Facility”, ASME Paper No. 2000-GT-480
[19] Ma, R., ,Morris, S. C. and Corke, T. C., 2006, “Design of a Transonic Research Turbine Facility”, AIAA Paper No. AIAA-2006-1311
[20] Stephan B., Gallus, H. E. and Niehuis, R., 2000, “Experimental Investigations of Tip Clearance Flow and Its Influence on Secondary Flows in a 1-1/2 Stage Axial Turbine”, ASME Paper No. 2000-GT-613
[21] König, S., Stoffel, B. and Schobeiri, M. T., 2009, “Experimental Investigation of the Clocking Effect in a 1.5-Stage Axial Turbine—Part I: Time-Averaged Results”, J. Turbomach., Vol. 131, No. 2, 021003
[22] Sell, M., Schlienger, J., Pfau, A., Treiber, M. and Abhari, R. S., 2001, “The 2-Stage Axial Turbine Test Facility ‘LISA’ ”, ASME Paper No. 2001-GT-0492
[23] Haldeman, C. W., Dunn, M. G., Barter, J. W., Green, B. R. and Bergholz, R. F., 2004, “Experimental Investigation of Vane Clocking in a One and 1/2 Stage High Pressure Turbine” ASME Paper No. GT2004-53477
[24] Numeca international, 2006, “AutoGrid V5-Automated Grid Generator for Turbomachinery”, User manual, Belgique

